WATER AND CO_2 ICE IN THE DARK DUNE SPOTS, RICHARDSON CRATER

F. Schmidt, *IDES, Université Paris-Sud 11; CNRS/INSU, Bâtiment 509, F91405,* **A. Kereszturi**, *Collegium Budapest, Institute for Advanced Study,* **M. Vincendon**, *Department of Geological Sciences, Brown University, Providence, Rhode Island, USA and IAS, Université Paris-Sud 11; CNRS/INSU, F91405*

Introduction:

Flow-like features [1] emanate from Dark Dune Spots [2] were observed in the Polar Regions, which may be formed with the help of interfacial water [3] or brines. Here we discuss the possibility of CO_2 ice, gypsum, liquid and solid water inside the large, easily observable spots at this terrain using spectroscopic and climate modeling arguments.

Methods:

We analyzed CRISM spectral data [4], with CAT-ENVI software [5] in Richardson crater (72°S, 179°E). During the work FRT hyperspectral images acquired in the long infrared region were used. After the photometric correction, default volcano scan 61C4 and New McGuire 2-wavelength (2007/1980) [6] filtering methods were used. Surface temperatures were derived from TES as average annual values with 3x8 km spatial resolution [7]. We focus on four units of the spots in Richardson crater dune (Fig. 1.): dark central part (core), their gray surrounding (ring), white "collar" (halo) and a bright average point on the winter frost covered dune field (undisturbed). The analyzed locations are visible in Fig. 2.

absorption band (microns)	component	characteristics
1.25	H_2O ice	Large-grained old water ice mainly, barely detectable for frost and cloud
1.5 (deepest)	H_2O ice	Wide min. between 1.38-1.8 with small asymmetry where the rise is steeper at the shorter wavelength [8]
2 (deepest)	H_2O & CO_2 ice	Wide between 1.9-2.1
2.2-2.5	H_2O ice	Decrease in reflectivity toward the longer wavelength
3	H_2O ice	Saturates when the path length of photons within H_2O ice exceeds a few micrometers
1.44	CO_2 gas	[8]
1.435	CO_2 ice	[11, 12]
2.281	CO_2 ice	[11, 12]
2.29 – 2.35	CO_2 ice	characteristic doublet absorption of CO_2 ice

Table 1. Absorption lines for H_2O and CO_2

Water ice spectroscopic identification using band ratio: A few μm of pure water ice at the surface of Mars creates characteristic near-IR absorption features several % deep (Table 2.). When mixed with other component (CO_2 ice, dust), the contrast of H_2O signatures is reduced: as little as 1% mixing concentration of water ice within CO_2 ice is however enough to be detectable in near-IR data [13]. When water ice is detected, it is however difficult to confirm the presence of surface water ice because atmospheric water ice particles in clouds may also produce resembling absorption feature. Important spectral lines are listed in Table 1. and the analyzed images in Table 2.

image no.	surf. temp. (K)	solar long. (deg.)	atm. H_2O cont. (microns)	local solar time
FRT000052BC	170	213.61	?	16.2
FRT000054E5	180	217.5	?	16.0
FRT00005FF6	266	248.72	11	15.7
FRT00007A6A	230	312.97	17	14.7

Table 2. The analyzed images of Richardson crater

Analyzing the change of spectra as the season passes by is visible in Fig. 3. for the dark spot in the period Ls=213-312.

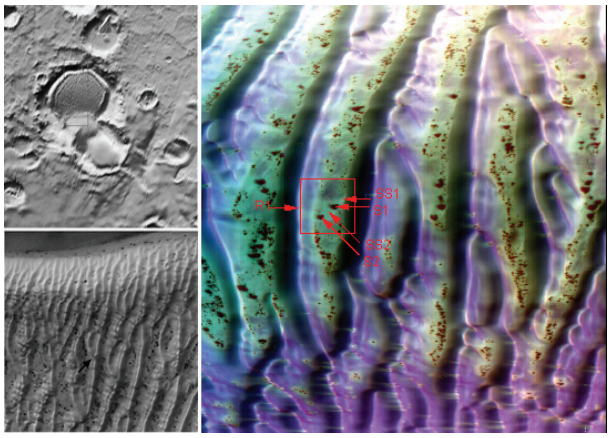

Fig. 1. Overview (left) and the analyzed locations (right) in Richardson crater.

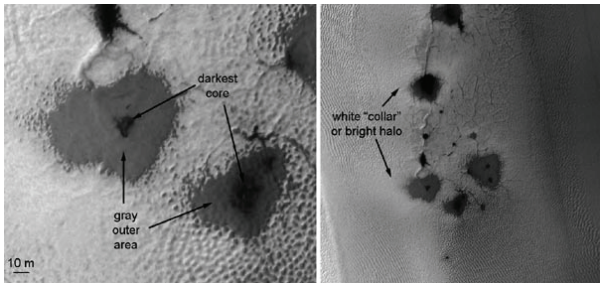

Fig 2: Unit types of the spots in Richardson crater on the HiRISE image # PSP_003175_1080. Dark cores and gray outer rings are visible in the left subset, while elongated and probably wind blown bright halos are present in the right subset

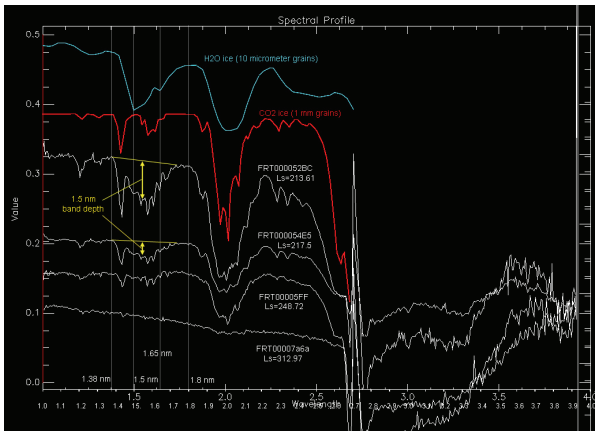

Fig 3. Spectral shapes of the spot and reference spectra of pure H_2O (blue) and CO_2 (red)

The range of Martian surface H_2O grain sizes is between 10 micrometer (frost) and 100 micrometer and even up to 1 mm (perennial ice cap) [14, 15], while atmospheric H_2O ice grains are smaller between 1 and 4 micrometer [16]. Based on the published results we choose the best features to identify large grain and as a result surface water ice particles the following (the largest grains producing the 1.25 micrometer line is not expected at the analyzed location as it may be composed of seasonal frost). We calculated both band ratios:

- H_2O ice centered at 1.5 micrometer normalized to 1.385 and 1.772 according to [8]. A strong absorption around 1,4 microns is also present both inside the spots and on the bright terrain too. At this spectral region two lines are very close to each other. The band values do not differ much inside and outside the spots and decreased as time passed by toward summer.
- CO_2 at 1.435 ice micrometer according to [8].

Results are plotted in Figure 5 on left side.

Water ice spectroscopic identification using linear unmixing: Water ice, liquid water and gypsum have really close spectra and thus the proper identification using band ratio is difficult (see Fig 4). We propose to use the Fully Constraint Least Square (FCLS) [17] linear unmixing technique with positive (non-negative) and sum-to-one constraints. This method also forces the abundances to be sparse (only a few non-zero abundances). This constrain will ensure to have only necessary spectral components in the results because not all spectra in the database are expected to present in the real data. We used the 6 endmembers spectra present in Figure 4. Results are plotted on the right side of Figure 5.

Discussion: The analyzed locations are visible in Fig. 2 at the end of southern winter on the HiRISE image acquired at Ls=213.61.

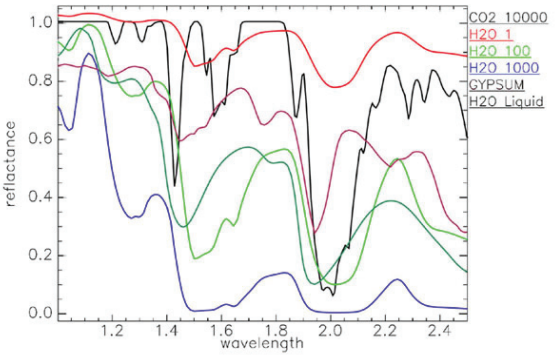

Fig. 4. Reference spectra used by FCLS to estimate the relative abundances for observed CRISM spectra. CO_2 ice at 10 cm grain size, H_2O ice at 1, 100 and 1000 microns have been modeled by a radiative transfer code [18] using optical constant recorded in the laboratory [20]. Both gypsum and liquid water have been acquired at LPG (Schmitt and Pommerol, unpublished). These spectra will be soon available online at http://ghosst.obs.ujf-grenoble.fr.

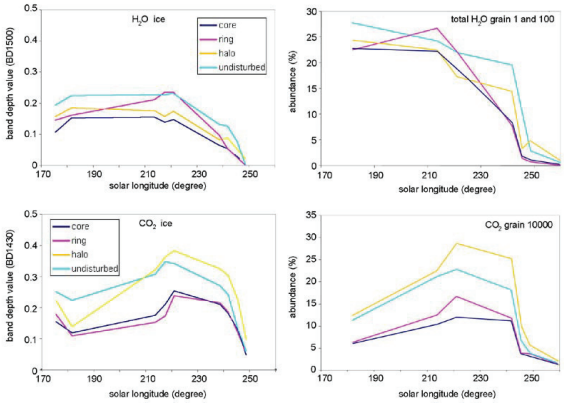

Fig. 5. Temporal changes of H_2O and CO_2 ice related band depth values (on the left) and spectral abundances estimated with the linear unmixing method FCLS (on the right) for different units (core: deep blue, ring: pink, halo: yellow, undisturbed ice: blue). The top right panel shows the sum of the abundances of water ice at different grain size (only

grain size of 1 and 100 microns are detected). The bottom right panel shows the abundance of CO_2 ice (only at 10 cm grain size). Top: H_2O ice. A general decrease can be seen, except for the gray ring, where an increase is present about Ls 215°. Bottom: CO_2 ice. The amount of CO_2 ice increases during early spring, with a stronger increase seen during the formation of the bright halo feature (yellow).

Climate modeling: Observations of water and CO_2 ice at Richardson crater are compared with the predictions of the Global Circulation Model developed at the Laboratoire de Météorologie Dynamique de Jussieu. This model is able to predict the water cycle of Mars and has been validated against available datasets [20 and reference herein]. The model computes the seasonal meteorology, notably the variations in water vapor and water ice precipitations, with a spatial sampling of 5x5° and a time step of half an hour. It is combined with a local energy balance code to predict the formation of ices on a given localized site with specific properties [21]. Three modeling hypotheses concerning local surface properties are shown in Fig. 6: (A) diamonds for standard parameters (flat surface, moderately bright ices), (B) stars for condensation on a 15° pole facing slope (to estimate the effect of local favorable conditions), (C) triangles for "dark" ice (albedo of 0.25 for both H_2O and CO_2 ice, a rough attempt to assess the impact of dust contamination of ice). These modeling predictions are compared to the presence or absence of ices at Richardson crater as a function of season as constrained from CRISM data, which show a general good agreement between data and model.

Results:

The general trend of the total H_2O ice spectral abundance (sum of H_2O with grain size of 1 and 100 µm) is compatible with the band ratio (Fig. 5 top). Water ice at 1 cm grain size is never detected. The dark core has the smallest mean grain size of the four units. The higher grain sizes are identified in the undisturbed terrain. Figure 12 suggests a general trend with increasing grain size until L_S= 220° and then decreasing until L_S=240°. These facts indicate that: (i) water ice is present with relative low grain size, consistent with seasonal ice; (ii) the grain size is evolving with time, which can be due to several mechanisms including resurfacing by sublimation, recondensation during the night, sublimation or deposition by geyser activity, grain metamorphism.

The results show that the spectral abundance of CO_2 ice is decreasing from 10% to 3% in agreement with band ratio (Fig. 5 bottom). Also, the fit of CO_2 ice bands is compatible with large grain size (10 cm) and possibly a translucent slab ice. The last observation image no. 6516 shows an estimated abundance of 0.06%, probably due to atmospheric residue.

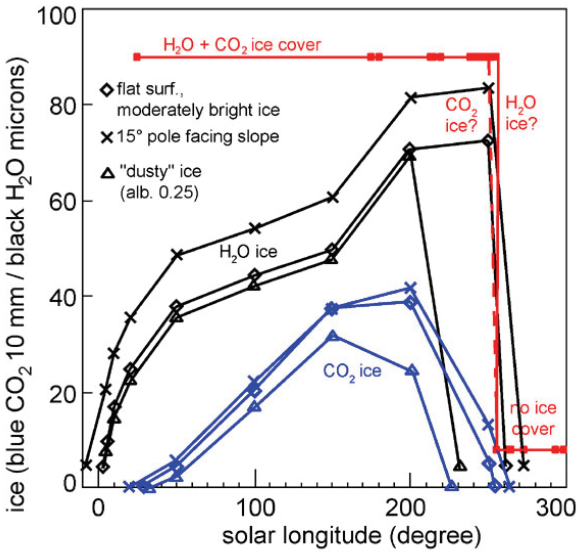

Fig. 6. Result of the model run on annual frost formation for H_2O ice (black) and CO_2 ice (blue), plus the observed presence of any kind of ice at the target location from CRISM data (red). It shows as a function of L_S (degree, horizontal axis) the cumulative thickness of CO_2 and H_2O ice condensed on the ground, on the vertical axis the thickness of H_2O and CO_2 are present using different scales, for CO_2 up to 40 cm and H_2O up to 80 µm thickness. Diamonds, triangles and crosses correspond to 3 hypotheses for model parameters related to ground properties (see text for details).

We have also included liquid water and gypsum and three linear unmixing scenarios: (1) without liquid nor gypsum (2) with liquid water only (3) with liquid water and gypsum. The rms is decreasing from model 1 to model 3 due to a slightly better fit of the 1.5 microns band. This tends to indicate that a spectral component with a water band shifted toward shorter wavelengths, such as gypsum or liquid water, could be present. Sulfates and/or liquid water have non-zero but very small abundances in six over the seven images considered (i.e.: for all observation except the last one at L_S=262.6°) in the "dark center" region, while it is almost never detected in the average terrain or in the bright halo. However, the retrieved abundances are low (< 3%), and differences in modeled spectra are not significant given the first order method employed here. Although the retrieval of a few % of species with a 1.45 microns band consistent with liquid water in the dark spots only is intriguing, no robust conclusions can be reached. Moreover, none of the ratio spectra show evidence for liquid water or gypsum. To assess more precisely the possible presence of liquid water and/or gypsum in CRISM spectra, a non-linear spectral inversion using radiative transfer model should be performed in the future.

In the climate model, Water ice accumulation starts before CO_2 ice at the beginning of fall, mainly due to snow precipitation of small grain size particles (more than 99% of the total water ice accumulation) that have condensed in the lower atmosphere according to the simulation. A thin layer of a few microns to a few 10s of microns thick H_2O ice below the CO_2 ice is expected according to model results, as noted by [22]. Then both ices condense simultaneously (H_2O inclusion within the CO_2 ice) 20 to 30° of L_S later. As a result we have a layered structure: only H_2O ice below, and CO_2 plus H_2O ice above. The ratio of H_2O ice in the upper layer depends on several factors, above all meteorological conditions and global atmospheric circulation, as during the CO_2 condensation in southern winter the average atmospheric vapor content reaches maximum supplied by the exposed northern permanent water ice cap. When cold CO_2 ice is present, it traps available water vapor. Ice disappears prior to the summer solstice even for favorable conditions. According to the model, water ice remains 5° to 10° of L_S later compared to CO_2. The contamination of ice by dust significantly decreases the stability of ice in spring, which sublimation is shifted by about 30° of L_S. According to the model, CO_2 ice disappears at L_S 220° for a moderately dark ice with a 0.25 albedo. This is consistent with the morphological and spectral analyses conducted above, showing that at a similar period (L_S 210°, see section 3.4) the grey ring is composed of an H_2O ice rich thin layer while surrounding areas are still covered by a thicker layer of CO_2 ice.

Conclusion:

At the area of gray rings on HiRISE images the bright icy layer that surrounds the spots is missing. Based on shadow length measurements an about 10 cm deep horizontal depression is present there, measured relative to the top of surrounding bright ice cover. These depressions were not present in earlier images, suggesting a formation due to the localized sublimation of the ice layer.

By analyzing CRISM images, HiRISE data and the result of a climate model, we propose a scenario for the formation and evolution of the ice layers in and around the dark dune spots of Richardson crater. During fall thin, tens of μm thick H_2O ice rich layer forms at the surface. 30° of L_S later a layer of CO_2 ice with inclusions of H_2O ice forms on top of it, and reach a thickness of a few tens of cm. During late winter / early spring the dark spots form, probably by geysers activity [23] in agreement with the large CO_2 grain size detected by the linear unmixing. A bright halo-like feature surrounds the spot and show stronger CO_2 signature than the undisturbed average ice-covered surface, suggesting CO_2 was refrozen there. The dark spots and the grey rings are located in a 10 cm thick depression compared to the surrounding bright, ice-rich layer. The dark center spot is ice-free at some places (but contain ice signatures in CRISM images due to spatial mixing and aerosols scattering). At L_S=210-230°, the gray ring area is covered by an enhanced thin layer of H_2O ice. The origin of H_2O may be from two sources: (i) condensation on the surface in autumn (before the formation of CO_2 layer) or during winter time (CO_2 layer acting as a clod trap) and exhumed by the differential sublimation of CO_2 and H_2O ice (ii) H_2O attached to the sand grains that are blown up by geyser activity and that fall at the surface around the spot.

The presence of water ice in physical contact with insolated dark dune material could lead to the formation of liquid water. In the gray ring area the water ice surrounds darker surface, where liquid interfacial water layer or brine [24] may form. We found no firm evidence for the presence of liquid water in near-IR spectra, although linear unmixing results show that the data are not inconsistent with a possible slight contribution (a few %) of liquid water in the dark core unit.

More details can be found in [25].

Acknowledgment:

This work has been supported by the ESA ECS-project No. 98076. This work was also supported by the Centre National d'Etudes Spatiales (CNES). We also acknowledge partial support from the Programme National de Planétologie (CNRS/INSU).

References:

[1] Kereszturi Icarus 201, 492-503. [2] Horvath 2009 Astrobiology 9(1) 90-103. [3] [Möhlmann 2008. Icarus 195, 131–139 [4] Murchie et al. 2007. JGR 11. 5D, CiteID E05S03, 10.1029/2006JE002682 [5] Morgan, Seelos, Murchie, 2009, CRISM Workshop [6] McGiure et al. 2008 IEEE Transactions 46/12. p. 4020-4040. [7] Christensen et al. 2001 JGR. 106, 23823-23872, Bandfield, Smith 2003 Icarus 161, 47-65. [8] Langevin et al. 2007, JGR 112 E08S12 [11] Grundy and Schmitt 1998 JGR 103 25809-25822, [12] Hansen 2005 JGR 110 E11003 [13] Schmitt, B. et al. COSPAR 2004 [14] Langevin et al. 2005 Science 307, 1581-1583, [15] Schmitt et al. 2005 LPSC 2326 [16] Clancy et al. JGR 108(E9) 5098 [17]Heinz and Chang, IEEE TGRS (2001) [18] Douté and Schmitt, JGR (1998) [19]Schmitt et al., Solar System Ices, Book (1998) [20] Forget, F et al. The Mars water cycle workshop, (2008) [21]Vincendon et al., JGR (2010) [22] Schmitt, B. et al., Third International Workshop on Mars Polar Energy Balance and the CO_2 Cycle (2009) [23] Kieffer et al., JGR (2000) [24] Mohlmann, Icarus (2004) [25] Kereszturi et al., PSS, (2010)